Study of the Distribution of Molecular Orientation in Highly Oriented Polyethylene by X-ray Diffraction

Claude-Paul Lafrance, Michel Pézolet, and Robert E. Prud'homme*

Department of Chemistry and Centre de Recherche en Sciences et Ingénierie des Macromolécules, Laval University, Québec, Québec, Canada G1K 7P4

Received January 29, 1991

ABSTRACT: High-density polyethylene (HDPE) cylindrical rods produced by ram extrusion were studied by wide-angle X-ray diffraction. Even order $\langle P_n(\cos\chi)\rangle$ coefficients of the Legendre polynomial series describing the orientation distribution of the 110, 200, 020, 011, 211, and 002 crystal planes were calculated from the X-ray data for n up to 32. It is shown that high order $\langle P_n(\cos\chi)\rangle$ values can be used to characterize the evolution of the orientation at high draw ratios, whereas the commonly used "orientation function", $\langle P_2(\cos\chi)\rangle$, reaches a constant value close to unity at draw ratios over approximately 12. The $\langle P_n(\cos\chi)\rangle_c$ values describing the c axis or molecular orientation distribution were computed from the different planes: the correlation between the coefficients thus calculated is excellent. It is concluded that the molecular orientation may be calculated from any arbitrary reflection for uniaxially oriented samples. Finally, the average $\langle P_n(\cos\chi)\rangle_c$ coefficients are used to compare the experimental distributions with those calculated from the pseudoaffine deformation model and from Gaussian, Lorentzian, and "most probable" distribution functions.

Introduction

Wide-angle X-ray diffraction (WAXD) is one of the most commonly used techniques for the investigation of the molecular orientation in semicrystalline polymers. It provides a direct sampling of the distribution $N(\chi,\psi)$ of orientation of the crystal axes with respect to the specimen reference directions (Figure 1).

A WAXD study of a given crystallographic reflection through the rotation of the χ and ψ angles at a fixed Bragg angle (2θ) gives a pole figure, which is a map of the density of the normal to the investigated crystal plane in the specimen macroscopic reference system. In samples exhibiting axial symmetry around the deformation direction (DD), a complete pole figure analysis is not required and a rotation of the sample around its polar angle (χ) is sufficient to reveal the distribution $N(\chi)$ of orientation of the crystal axis.

Graphical representations such as pole figures or polar scans yield detailed information on the orientation distribution of a particular crystal plane. However, it is necessary to relate data from different crystallographic reflections to obtain an overall picture of the molecular orientation. Also, reflections from planes that are perpendicular to the polymer chains (00l) are frequently absent or too weak to be analyzed with sufficient accuracy. Then, the molecular orientation distribution has to be calculated from measurements made on other crystal planes.

Roe and Krigbaum have described the method of pole figure inversion to calculate the orientation of any crystal plane from the measured distributions of different hkl reflections.[1-3] Due to its complexity, this analysis has been so far limited to studies of the deformation mechanism of polyethylene[2,4-6] and poly(ethylene terephthalate)[7] at low draw ratios. Moreover, in order to get sufficient accuracy, measurements have to be made on several crystallographic planes, whose number increases with the extent of orientation.

The detailed information given by the pole figure inversion method is seldom necessary, particularly when the change in polymer morphology from a spherulitic to a fibrous structure has been completed. The analytical index that is most often used to characterize the extent

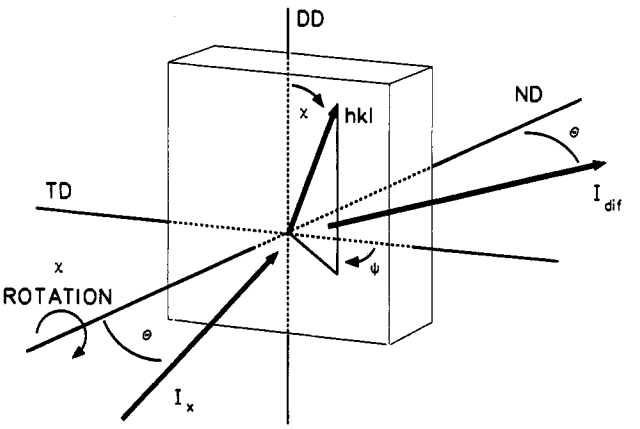

Figure 1. Angles χ and ψ defining the position of the normal to a given hkl crystal plane in the sample reference system [DD, deformation (drawing, rolling or extrusion) direction or fiber axis; ND, normal direction; TD, transverse direction; I_x, incident X-ray beam; I_{dif}, hkl diffracted intensity].

of orientation is the so-called "orientation function", f. This function, which was first proposed by Hermans,[8,9] is defined as the mean coefficient of the second-order Legendre polynomial, $P_2(\cos\chi)$:

$$f = \langle P_2(\cos\chi)\rangle = (3\langle\cos^2\chi\rangle - 1)/2 \qquad (1)$$

Its limiting values, taking $\chi = 0°$ as the deformation direction, are −0.5 for a perfect perpendicular orientation and +1.0 for a perfect parallel orientation. An unoriented material gives $\langle P_2\rangle = 0$. (In the following pages, the notation $\langle P_n\rangle$ will be used to represent the mean coefficient of the nth order Legendre polynomial. The brackets mean that an average is taken over all orientations.)

The use of $\langle P_2\rangle$ as an orientation index has two advantages. First, all characterization methods commonly used to study the orientation lead to the measurement of $\langle P_2\rangle$, for either the crystalline or the amorphous phase and sometimes for both. Second, following the data treatments proposed by Wilchinsky[10,11] or Sack,[12] the calculation of $\langle P_2\rangle$ for axes that cannot be observed directly is possible from $\langle P_2\rangle$ values obtained from other crystal planes.

0024-9297/91/2224-4948$02.50/0

On the other hand, $\langle P_2 \rangle$ is bounded to the mathematical form of the second-order Legendre polynomial, which is a maximum at $\chi = 0°$ and a minimum at $\chi = 90°$. It is not suitable for the characterization of orientation distributions that are not aligned along these axes. For the crystalline phase, the use of $\langle P_2 \rangle$ raises another problem. During the transformation from the spherulitic to the fibrillar morphology, which for polyethylene is completed at draw ratios around 10,[13] $\langle P_2 \rangle$ increases rapidly to values over 0.95 and remains constant afterward. It then becomes almost impossible to follow the evolution of the orientation with further deformation of the material.

Therefore, some authors have successfully used higher order Legendre polynomial coefficients to characterize highly oriented polymers.[14,15] Surprisingly, this has not become a common practice, and most X-ray studies of polymers are still limited to the determination of $\langle P_2 \rangle$. This situation may arise from the belief that the coefficients calculated with high powers of the cosine function are subjected to a large experimental error. Moreover, the $\langle P_n \rangle$ values measured for an arbitrary crystal reflection may not appear, at first glance, to give significant information on the molecular orientation distribution.

In this study, calculations of $\langle P_n \rangle$ coefficients up to $n = 32$ were made from WAXD measurements on a high-density polyethylene (HDPE). Different $hk0$, hkl, and $00l$ planes were investigated and $\langle P_n \rangle$ values calculated for each of these crystal planes. The $\langle P_n \rangle_c$ coefficients corresponding to the orientation distribution of the molecular chains were also calculated from these different reflections using a relationship suggested by Lovell and Mitchell.[16] The validity of $\langle P_n \rangle_c$ values obtained from arbitrary crystal planes to express the molecular chain distribution will be discussed. Finally, the average $\langle P_n \rangle_c$ values will be used to compare the experimental orientation distributions with the pseudoaffine model and with mathematical distribution functions.

Experimental Section

Samples. The HDPE samples used in this study were cylindrical rods made of Du Pont "SCLAIR 2909" resin (M_n = 16 400, M_w = 56 500). The rods were produced from preheated (120 °C) billets by ram extrusion at 145–155 °C through conical dies. Draw ratios (λ) of 6, 8, 12, 16, and 20 were obtained, with rod diameters ranging from 1.40 to 0.75 cm. For the X-ray work, 1,2-mm-thick platelets were cut along the extrusion direction in the center of the rods. These platelets had smooth surfaces and were translucent.

X-ray Measurements. Wide-angle X-ray diffraction measurements were made by using nickel-filtered Cu Kα radiation (0.154 187 nm) produced by a Rigaku rotating-anode X-ray generator (Rotaflex RU-200BH) operated at 50–55 kV and 160–190 mA. The collimation was achieved by using a Soller slit and a 1.0-mm pinhole. The detection of the diffracted intensity was provided by a scintillation counter coupled with a pulse-height analyzer.

All scans were recorded with the symmetrical transmission technique, the normal to the sample surface being positioned at an angle θ with respect to the incident X-ray beam and the detector at an angle 2θ (Figure 1). During the orientation measurements, the polar angle (χ) rotation of the sample (rotation of the sample around the normal to its surface) was performed from −90° to +90° at a rate of 30 °/min, $\chi = 0°$ corresponding to the extrusion direction (DD). Measurements were taken at 0.5° intervals, using 1.5° and 0.25° slits for 2θ and polar angle resolution, respectively.

Crystallographic Planes of Interest and Background Evaluation. In this work, the orientation of the HDPE crystalline phase was investigated through six hkl reflections of its orthorhombic unit cell. Crystallographic parameters for the measured 110, 200, 020, 011, 211, and 002 planes and for other reflections that were not resolved from the former ones are listed in Table I. The unit cell dimensions (a = 0.741, b = 0.492, and c = 0.2538 nm) were calculated in order to get the best fit with the measured 2θ angles. They correlate very well with values given in the literature for linear HDPE.[17-19] The interplanar distance "d" and the angle "ϕ" between a given plane normal and the c axis were calculated by using the relationships

$$d = [(h/a)^2 + (k/b)^2 + (l/c)^2]^{-1/2} \quad (2)$$

and

$$\phi = \arccos(ld/c) \quad (3)$$

For all samples, $\theta/2\theta$ diffractometer scans were taken in the angular ranges 15–55° and 70–80°, at polar angles of 0, 27, 41, 60, and 90°. The position of the diffraction maximum for each reflection of interest was determined from these curves, and the polar scans were then performed at these 2θ values. The position of the 2θ peaks did not vary with the draw ratio.

As a representative example, Bragg angle scans obtained for the $\lambda = 12$ sample are shown in Figures 2 and 3, while Figure 4 displays the polar scans of the six reflections that were investigated. The 2θ and polar scans were used to detect and identify reflections overlapping with those under investigation. Aside from unresolved peaks of the orthorhombic phase, diffraction caused by the amorphous and monoclinic phases could interfere with the orientation calculations. As may be estimated visually from Figure 2, the intensity of the amorphous halo (centered around $2\theta = 20°$) is very weak for these samples. Nevertheless, it could be responsible for the slight curvature of the background of the 110 polar scan (Figure 4). It is also well-known that a certain amount of monoclinic phase (a = 0.809, b = 0.479, c = 0.253 nm, γ = 107.9°) is produced when PE is submitted to compression.[20,21] Its presence is ascertained by the 010 reflection that appears as a shoulder ($2\theta = 19.6°$) on the 110 peak of the orthorhombic phase (see Figure 2). The other strong reflections of the monoclinic phase (200, 210, and 210 at 23.1°, 25.3°, and 34.8°, respectively) were not observed, indicating that the amount of this phase is low. Moreover, as the c axis (parallel to the molecular chains) is the unique axis of the monoclinic unit cell, the orientation behaviour of the monoclinic crystals should be similar to that of the orthorhombic crystals. Thus, the $hk0$ reflections of the monoclinic phase should orient toward the equator ($\chi = 90°$), along with the orthorhombic 110 and 200 peaks that they overlap, and should not cause any appreciable broadening of the polar scans peaks.

Table I
Experimental and Calculated Bragg Angles (2θ), Interplanar Distances (d), and Angles between the Crystal Plane Normals and the Deformation Direction (ϕ) for the Polyethylene Orthorhombic Unit Cell (a = 0.741, b = 0.492, and c = 0.2538 nm)

hkl[a]	$2\theta_{exptl}$, deg	$2\theta_{calc}$, deg	d, nm	ϕ, deg
amorphous halo	17–23	15–25		
M010	19.5	19.47	0.4558	90.0
*110	21.65	21.67	0.4102	90.0
*200	24.00	24.02	0.3705	90.0
M001	35.7	35.4	0.2538	0.0
*020	36.53	36.49	0.2463	90.0
120	38.55	38.52	0.2337	90.0
*011	39.98	39.96	0.2256	27.3
310	40.90	40.87	0.2208	90.0
111	41.88	41.85	0.2158	31.8
220	44.20	44.16	0.2051	90.0
*211	47.19	47.16	0.1927	40.6
400	49.24	49.18	0.1853	90.0
231	73.36	73.27	0.1292	59.4
421	74.16	74.15	0.1279	59.3
520	74.84	74.76	0.1270	90.0
*002	74.80	74.82	0.1269	0.0
511	76.94	76.98	0.1239	60.8
600	77.7	77.25	0.1235	90.0
040	77.7	77.53	0.1231	90.0
430	77.7	77.72	0.1229	90.0

[a] M indicates a reflection of the monoclinic phase (see text). An asterisk indicates the reflections that were investigated.

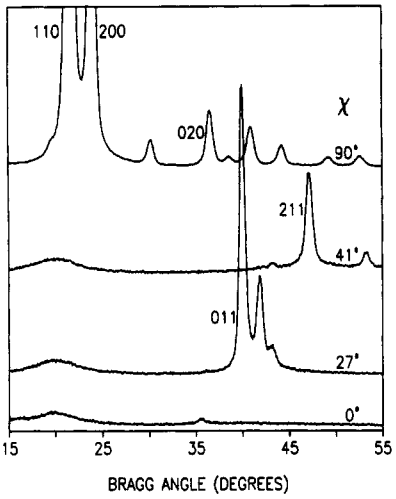

Figure 2. X-ray intensity measured as a function of the Bragg angle for the λ = 12 sample at different polar angles, χ. The intensity scale of the curve measured at χ = 90° is reduced by a factor of 4 compared to the other ones.

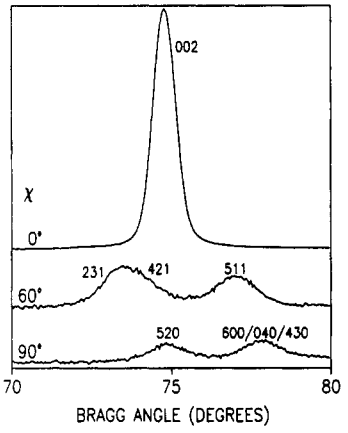

Figure 3. X-ray intensity measured as a function of the Bragg angle for the λ = 12 sample at different polar angles, χ. The intensity scale of the curve measured at χ = 0° is reduced by a factor of 15 compared to the other ones.

The 020, 011, 211, and 002 polar scans all showed the presence of unresolved reflections, appearing at 2θ angles near the peak position of the planes studied. However, the polar peaks of interest could be easily resolved from those due to the overlapping reflections, owing to the high orientation of the samples and to their narrow orientation distributions. As is observed in Figure 4, the polar peak of a given reflection is centered around its φ angle position (see Table I) and its intensity falls to a flat base line before the onset of any unresolved peak. For these planes the calculations were thus made on limited angular ranges, in order to exclude contributions from the unresolved reflections (see the Appendix).

Prior to the calculations, the polar scan curves were smoothed by using a moving-average five-point method. To avoid any deformation of the polar peak, the smoothing was conducted on the "background" part of the scan uniquely, at least 15° away from the peak maximum.

The value of the background intensity for each reflection (caused by amorphous and air scattering) was taken equal to the minimum intensity recorded in the polar scan. For the λ = 6 and 8 samples, the background intensity was also calculated from the base lines drawn in the five 2θ scans made at different polar angles. The lowest value thus measured for each reflection at its peak 2θ position was in all cases equal, within experimental error, to that obtained from the polar scans.

⟨P_n⟩ Coefficients and Orientation Distribution Calculations. The corrected intensity at a polar angle χ, $I^*(\chi)$, was obtained by subtracting the background from the average of the two experimental values measured at −χ and +χ. The

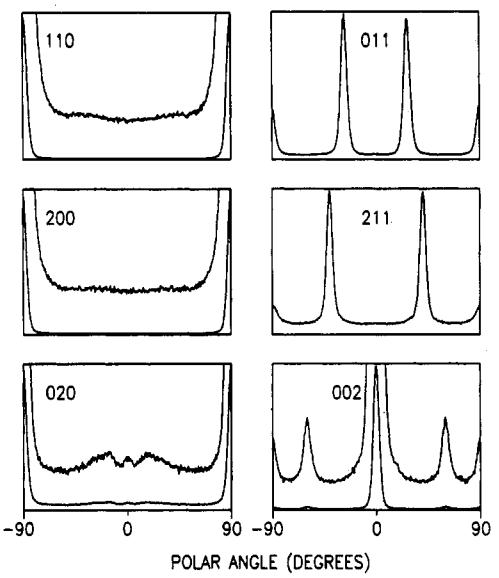

Figure 4. X-ray intensity measured as a function of the polar angle with the λ = 12 sample for six crystal planes.

normalized intensity distribution, $q(\chi)$, was then computed from the relation

$$q(\chi) = \frac{I^*(\chi)}{\int_0^{90} I^*(\chi) \sin \chi \, d\chi} \tag{4}$$

The ⟨P_n⟩ coefficients were calculated for n = 2–32 through the equation[22]

$$\langle P_n \rangle = \int_0^{90} q(\chi) \, P_n(\cos \chi) \sin \chi \, d\chi \tag{5}$$

using the Tallqvist[23] expressions of the Legendre polynomials $P_n(\cos \chi)$. The odd coefficients are equal to zero for samples possessing a plane of symmetry perpendicular to the deformation direction, so only even ⟨P_n⟩ values were computed. The numerical integration of eqs 4 and 5 was performed by using Simpson's rule.

The orientation distribution function, $\rho_t(\chi)$, of a given reflection may be reconstructed by insertion of the ⟨P_n⟩ coefficients up to $n = t$ in the relation

$$\rho_t(\chi) = \sum_{n=0}^{t} (n + 1/2)\langle P_n \rangle P_n(\cos \chi) \tag{6}$$

Distribution curves obtained by using terms of the series up to n = 8, 20, and 32 were compared to the normalized intensity distribution $q(\chi)$. The difference between the experimental curve and the distributions calculated by using ⟨P_n⟩ values up to $n = t$, σ_t, hereafter called the standard deviation of the distribution function, was computed by

$$\sigma_t = \left(\frac{\int_0^{90} [q(\chi) - \rho_t(\chi)]^2 \sin \chi \, d\chi}{\int_0^{90} [q(\chi)]^2 \sin \chi \, d\chi} \right)^{1/2} \tag{7}$$

⟨P_n⟩ values calculated from the 002 plane characterize the molecular chain orientation distribution, since the crystal c axis is parallel to the chains. The results obtained from other planes can be transformed into ⟨P_n⟩$_c$ coefficients relative to the c axis orientation through[16]

$$\langle P_n \rangle_c = \langle P_n \rangle_{hkl} / P_n(\cos \phi_{hkl}) \tag{8}$$

where ϕ_{hkl} is the angle between the normal to the hkl plane and the c axis (see Table I). This equation holds if the orientation distribution possesses cylindrical symmetry around the deformation direction.[16,22] For the ⟨P_2⟩ coefficient calculated from a $hk0$ plane, eq 8 is equivalent to the well-known Wilchinsky relation

Table II
Selected $\langle P_n \rangle$ Values Calculated from *hk*0 Planes for the λ = 6, 12, and 20 Rods

	$\langle P_n(\cos\chi)\rangle$						
*hk*0	*n* = 2	*n* = 4	*n* = 6	*n* = 8	*n* = 16	*n* = 24	*n* = 32
λ = 6							
110	−0.44	0.26	−0.16	0.09	0.01	0.00	0.00
200	−0.46	0.29	−0.20	0.13	0.03	0.00	0.00
020[a]	−0.45	0.26	−0.16	0.10	0.02	0.00	0.00
λ = 12							
110	−0.49	0.35	−0.28	0.23	0.11	0.05	0.02
200	−0.49	0.36	−0.28	0.24	0.13	0.07	0.04
020[a]	−0.49	0.35	−0.27	0.23	0.12	0.07	0.04
λ = 20							
110	−0.49	0.36	−0.29	0.24	0.14	0.08	0.05
200	−0.49	0.36	−0.29	0.24	0.15	0.09	0.06
020[a]	−0.49	0.35	−0.29	0.24	0.15	0.10	0.07
theoretical perfect orientation at χ = 90°	−0.50	0.38	−0.31	0.27	0.20	0.15	0.14

[a] Integrals of eqs 4 and 5 evaluated between χ = 45 and 90° (see the Appendix).

for $\langle \cos^2\chi \rangle$ in the case of uniaxial orientation (orthorhombic unit cell)[11,24]

$$\langle \cos^2\chi \rangle_c = 1 - 2\langle \cos^2\chi \rangle_{hk0} \quad (9)$$

which in terms of $\langle P_2 \rangle$ can be converted to

$$\langle P_2 \rangle_c = -2\langle P_2 \rangle_{hk0} \quad (10)$$

Results and Discussion

$\langle P_n \rangle$ Coefficients from *hk*0 and *hkl* Planes. Table II gives some of the $\langle P_n \rangle$ values calculated from equatorial (*hk*0) planes for the λ = 6, 12, and 20 rods. $\langle P_n \rangle$ values for the λ = 6 samples indicate a slightly narrower orientation distribution of the *a* axis than of the *b* axis around χ = 90°. This result is in agreement with the observations of Stein[25] and with deformation models proposed by Pietralla[26] and by Kawai and co-workers.[4,5] The distribution functions calculated by using eq 6 with $\langle P_n \rangle$ coefficients up to 8, 20, and 43 are reproduced in Figure 5 for the 200 reflection. It is observed that the distribution obtained by ending the series at $\langle P_8 \rangle$ is broader than the experimental intensity curve. The addition of terms up to *n* = 20 gives a distribution that is almost identical with the experimental one, with, however, small-amplitude oscillations around ρ(χ) = 0 in the low density region. These oscillations, caused by the series termination whenever the higher $\langle P_n \rangle$ coefficients are nonnegligible, are removed when terms up to $\langle P_{32} \rangle$ are included. In the case of the λ = 6 sample, the *n* = 32 series calculated for the three *hk*0 planes give distribution functions that match almost perfectly with the experimental curves, with a standard deviation (eq 7) below 1.4%.

In the case of the λ = 20 sample, the calculated distribution function ρ(χ) is broader than the experimental one, even with terms up to $\langle P_{32} \rangle$ (Figure 5). Similar results were obtained for the 110 and 020 planes. The value of the standard deviation σ_{32} between the measured distribution and $\rho_{32}(\chi)$ is plotted as a function of λ in Figure 6. For samples of low draw ratios (λ ≤ 8), the agreement between the experimental and calculated distribution is excellent, with σ_{32} below 4% for all *hk*0 planes. However, at higher draw ratios, the $\langle P_n \rangle$ coefficients over *n* = 32 are no longer negligible, and the series termination error increases.

For the λ = 12 and 20 rods, the $\langle P_2 \rangle$ values (Table II) are very close to the −0.50 theoretical value that corresponds to a perfect orientation at χ = 90°, indicating a very narrow distribution of the *a* and *b* axis around this angle. The finite width of the experimental distribution shows up by the increasing difference between the calculated and the theoretical $\langle P_n \rangle$ values as *n* gets higher. This demonstrates that the characterization of narrow X-ray intensity distributions, as those measured on highly oriented samples, must involve the higher degree Legendre polynomials, which possess lobes with a width comparable to the observed distribution. In other words, the $\langle P_2 \rangle$ and $\langle P_4 \rangle$ coefficients fail to distinguish between the extent of orientation of λ = 12 and λ = 20 rods while higher $\langle P_n \rangle$ results reveal a significant difference.

The $\langle P_n \rangle$ calculations from the 011 and 211 polar scans have been made in the χ = 0–65° and χ = 0–70° ranges, respectively, in order to remove the equatorial peaks due

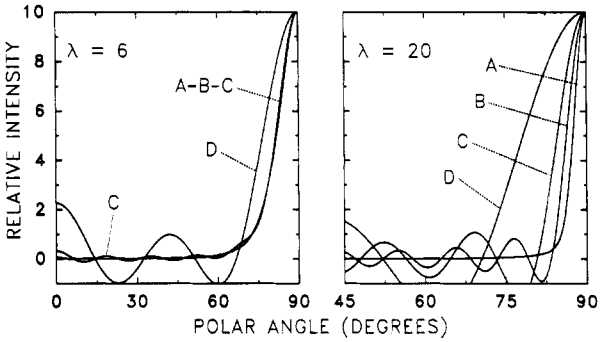

Figure 5. Normalized intensity distribution $q(\chi)$ (A) and distribution function $\rho(\chi)$ calculated using $\langle P_n \rangle$ coefficients up to *n* = 32 (B), 20 (C), and 8 (D) for the 200 reflection of the λ = 6 and 20 samples.

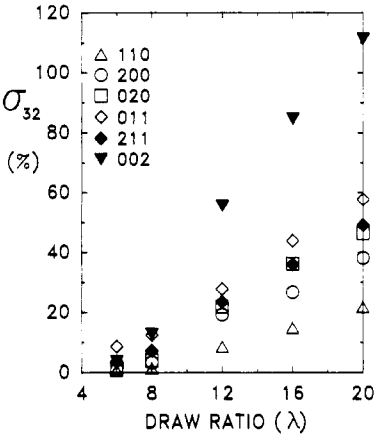

Figure 6. Standard deviation σ_{32} between the normalized intensity distribution $q(\chi)$ and the distribution function calculated by using terms up to $\langle P_{32} \rangle$ as a function of λ for the different crystal planes investigated.

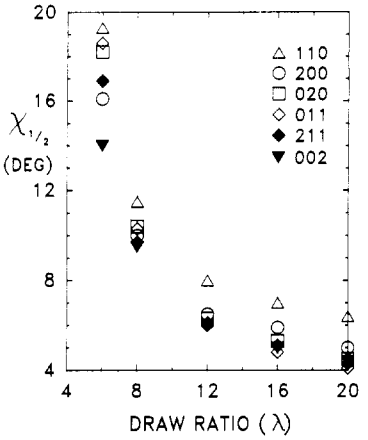

Figure 7. Full-width at half-height, $\chi_{1/2}$, of the polar peaks as a function of λ for the different crystal planes investigated.

to the overlapping reflections (see Figure 4 and Table I). As shown in Figure 6, a comparison of the calculated distribution functions with the experimental curves gives σ_{32} values that are similar to those obtained from *hk*0 planes.

The polar scan peaks may also be characterized by their full-width at half-height, $\chi_{1/2}$, as shown in Figure 7. This simple parameter, which has seldom been employed,[27-29] is much more useful to study the orientation of highly oriented samples than the commonly used orientation function: whereas the value of $\langle P_2 \rangle$ levels off at draw ratios over 12, the full-width at half-height still indicates an increase in orientation. The results presented in Figures 6 and 7 for the *hk*0 planes also demonstrate that the series termination error is inversely proportional to the width of the polar scan peak. This explains the lower σ_{32} values obtained with the 110 reflection, since this peak is broader than the other ones.

It is interesting to note that at low draw ratios the width of the 200 reflection is smaller than that of the 020 reflection, the situation being reversed at higher draw ratios. This effect may be explained either by a deformation mechanism where the orientation of the *a* axis toward $\chi = 90°$ is faster than the orientation of the *b* axis[26] or by a relaxation mechanism occurring through rotation of the crystals around the *a* axis. As rods of lower draw ratios possess a larger diameter than the other ones, some relaxation may take place in the center of these bigger rods, while the orientation in the smaller rods is frozen in as they leave the die.

$\langle P_n \rangle$ Coefficients from the 002 Reflection. For the 002 reflection, the $\langle P_n \rangle$ coefficients were calculated in the $\chi = 0$–40° integration range, as the onset of the 231/421/511 peak is located around $\chi = 45°$ (Figure 4). The distribution functions $\rho(\chi)$ calculated for the 002 reflection of the λ = 6 and 20 rods are shown in Figure 8. As with the equatorial reflections, the fit between the $\rho_{20}(\chi)$ and the $\rho_{32}(\chi)$ functions, on the one hand, and the experimental curve, on the other hand, is good for the λ = 6 sample, with σ values of 17% and 3.6%, respectively. For the λ = 8 sample the $\rho_{32}(\chi)$ function still gives a good agreement with the measured distribution, the σ_{32} = 13% being associated with small-amplitude oscillations in the low density region (curves not shown). At high extrusion ratios, even the $\rho_{32}(\chi)$ function is broader than the experimental curve, the σ_{32} value becoming higher than 110% at λ = 20 (see Figure 6). For a similar full-width at half-height, the discrepancy between the calculated and experimental distributions is larger for the 002 reflection than for the *hk*0 and *hkl* planes. This difference is due to the shape

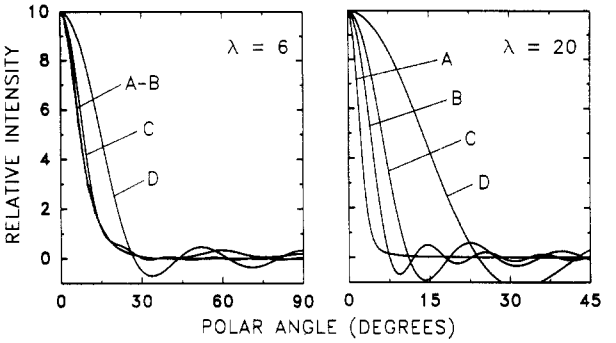

Figure 8. Normalized intensity distribution $q(\chi)$ (A) and distribution functions $\rho(\chi)$ calculated by using $\langle P_n \rangle$ coefficients up to n = 32 (B), 20 (C), and 8 (D) for the 002 reflection of the λ = 6 and 20 samples.

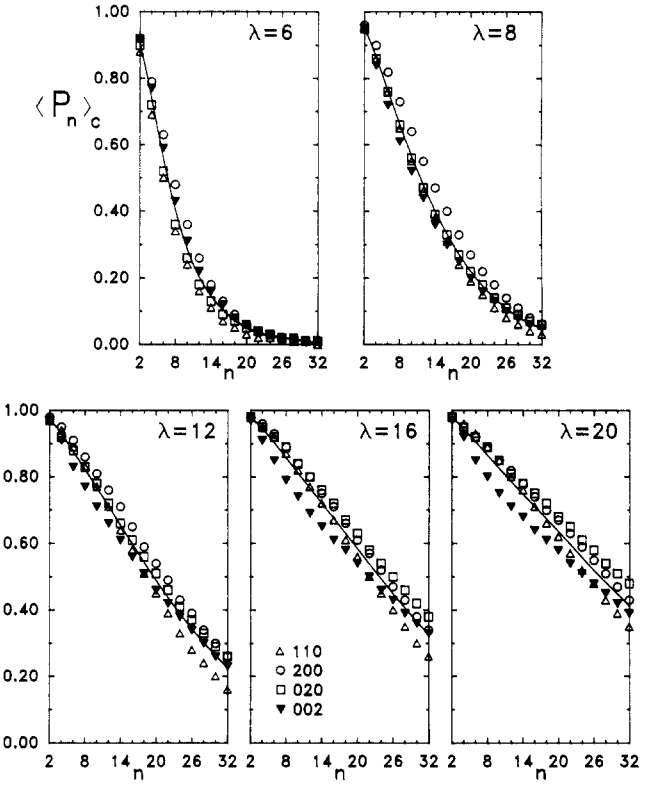

Figure 9. Sets of $\langle P_n \rangle_c$ coefficients characterizing the molecular chain orientation, calculated from *hk*0 and 002 planes for five different HDPE extruded rods.

of the Legendre polynomial curves, where the main lobe located at $\chi = 0°$ is broader than the other ones (see the Appendix).

The $\langle P_n \rangle$ values calculated from the 002 reflection give a direct characterization of the molecular orientation distribution, since the *c* axis of the polyethylene crystals is parallel to the chains ($\langle P_n \rangle_{002} = \langle P_n \rangle_c$). In the next section, we will compare the $\langle P_n \rangle_c$ coefficients obtained from the other planes using eq 8 with these results.

Comparison of $\langle P_n \rangle_c$ Coefficients Calculated from Different Planes. As seen in Figure 9, for all samples investigated, the sets of $\langle P_n \rangle_c$ coefficients obtained from the 002 and *hk*0 planes are in very good agreement. This may be considered as a confirmation of the cylindrical symmetry of the molecular distribution around the deformation direction, because any deviation from this symmetry should result in a discrepancy between the $\langle P_n \rangle_c$ calculated from eq 8. The fact that the coefficients from the 110 reflection are slightly lower than the other ones for $n \geq 20$ may be explained by the overlap of the

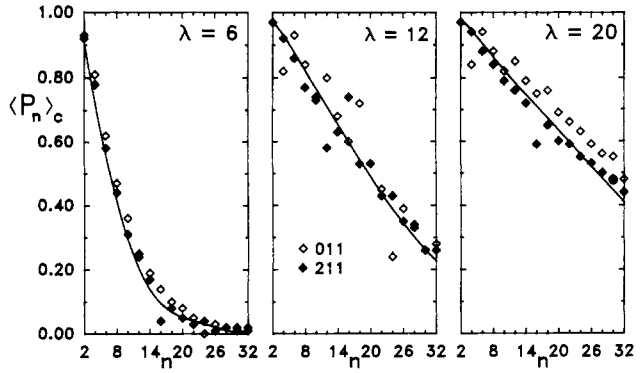

Figure 10. Sets of $\langle P_n \rangle_c$ coefficients characterizing the molecular chain orientation, calculated from *hkl* planes for the λ = 6, 12, and 20 HDPE extruded rods (the full curve is that obtained with *hk*0 and 002 planes, Figure 9).

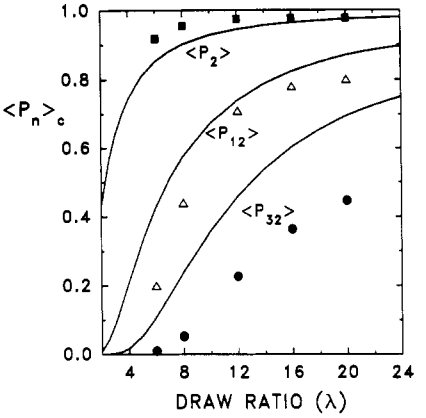

Figure 11. Average $\langle P_n \rangle_c$ values obtained with the five HDPE rods, for n = 2, 12, and 32, and curves predicted by the pseudoaffine deformation scheme for the same coefficients.

amorphous halo with this reflection. Measurements made by Wilchinsky have shown that the amorphous halo of drawn PE concentrates in a diffuse arc toward the equator.[24] In the 110 polar scans, it appears as a shoulder overlapping with the tail of the main peak. Although the weak intensity of this component does not influence the lower $\langle P_n \rangle$ coefficients, it seems to affect the convolution with the narrower lobes of the higher Legendre polynomials.

It should also be noticed from Figure 9 that if the $\langle P_n \rangle_c$ values do not vary appreciably for the different samples studied, the higher coefficients show a significant increase with λ, even at the highest draw ratios. This fact clearly demonstrates that when the orientation function $\langle P_2 \rangle$ reaches a constant value close to unity, it is still possible to characterize the evolution of the molecular orientation in the crystalline phase using the higher $\langle P_n \rangle$ or $\langle P_n \rangle_c$ coefficients.

The $\langle P_n \rangle_c$ coefficients calculated from *hkl* planes agree well with the curve drawn from the results of *hk*0 and 002 planes, as shown in Figure 10, but exhibit at the same time some scattering. The reason for that behavior lies in the shape of the Legendre polynomials (see the Appendix). The peak maximum of *hkl* planes is located at polar angles where some of the polynomials exhibit a rapid variation. For example, the polynomials of degrees n = 4, 6, 12, 18, and 24 change sign at about $\chi = 27.3°$, where the 011 reflection is centered. The $\langle P_n \rangle$ coefficients computed for these n values are thus very small and do not influence strongly the distribution functions $\rho(\chi)$ for the 011 planes. However, in the calculation of the corresponding $\langle P_n \rangle_c$ values through eq 8, the $\langle P_n \rangle$ coefficient is divided by a quantity that is close to zero, and the result thus bears an important uncertainty, as shown in Figure 10.

Comparison of Experimental $\langle P_n \rangle_c$ Coefficients with the Pseudoaffine Deformation Model. The pseudoaffine deformation scheme, originally proposed by Kratky,[30] is often used to model the development of orientation in drawn polymers.[31-39] This deformation model assumes that the polymer is a two-phase system, composed of transversely isotropic rigid units embedded in a deformable matrix. The evolution of orientation proceeds through the rotation of the unique axis of these rigid "floating rods" toward the elongation direction. For uniaxial deformation, the resulting orientation distribution of the molecular axis is given by[31,39]

$$q(\chi) = \frac{\lambda^3}{2\pi(\cos^2\chi + \lambda^3 \sin^2\chi)^{3/2}} \qquad (11)$$

The pseudoaffine mechanism has been particularly successful in describing the evolution of birefringence in crystalline polymers and the shape of the orientation–strain relationship in glassy polymers.[38,39]

Figure 11 compares the average $\langle P_2 \rangle_c$, $\langle P_{12} \rangle_c$, and $\langle P_{32} \rangle_c$ values measured in this study to the curves for the same coefficients calculated from the pseudoaffine distribution. It is seen that the experimental $\langle P_2 \rangle_c$ results are higher than those predicted by the model, as has also been reported from X-ray measurements on low and high density polyethylene[33] and on polypropylene.[36] On the other hand, the experimental coefficients are below the corresponding pseudoaffine curve for $\langle P_8 \rangle_c$ and higher values. These apparently contradictory results emphasize the frequently misinterpreted significance of the $\langle P_2 \rangle$ values, which are too often considered as an absolute index of orientation. It should be kept in mind that $\langle P_2 \rangle$ is the first coefficient of a series distribution function and that distributions of different width and centered at different angles may possess the same $\langle P_2 \rangle$.[40] Thus the knowledge of higher order $\langle P_n \rangle$ coefficients is not merely indicative of the "degree" of orientation but serves to characterize the shape and the peak position of the distribution. For example, the polar scan peaks observed with the λ = 6 sample have a full-width at half-height of at least 14°, as compared to 5.9° for the pseudoaffine distribution, which explains the higher values of the model $\langle P_n \rangle_c$ coefficients for $n \geq 8$. Still, the theoretical $\langle P_2 \rangle_c$ to $\langle P_8 \rangle_c$ values are smaller than those measured because the tail in their distribution curve decreases more slowly than that in the experimental curve.

The high experimental values of $\langle P_2 \rangle_c$ at λ = 6 and 8 are probably related to the transition from the spherulitic to the fibrillar structure. Once this transformation is completed, the orientation of the fibrils could be expected to follow the floating rod model. However, it is observed that the increase of the experimental $\langle P_n \rangle_c$ coefficients occurs more slowly than predicted by the pseudoaffine scheme. This mechanism thus seems inadequate to describe the evolution of the crystalline orientation distribution of the samples investigated.

Comparison of Experimental and Calculated Distribution Functions. WAXD is the only experimental method that enables the calculation of all the $\langle P_n \rangle$ coefficients. Other techniques are generally limited to $\langle P_2 \rangle$ and $\langle P_4 \rangle$. Clearly, the first terms of the series distribution function (eq 6) are unable to reproduce the shape of the molecular orientation distribution, especially with highly oriented specimens. It would therefore be interesting to find a mathematical function that would give a good approximation to the experimental distribu-

Table III
Full-Width at Half-Height, $\chi_{1/2}$, and Selected $\langle P_n \rangle_c$ Coefficients for the Experimental Orientation Distribution of Samples λ = 6, 12, and 20 and for Gaussian, Lorentzian, and MPD Functions of Similar $\langle P_2 \rangle_c$ and $\langle P_4 \rangle_c$ Values

function	$\chi_{1/2}$,[a] deg	$\langle P_n \rangle_c$ n = 2	n = 4	n = 6	n = 8	n = 16	n = 24	n = 32
λ = 6								
expt	14.1	0.92	0.76	0.58	0.43	0.12	0.03	0.01
Gauss	22.4	0.92	0.76	0.56	0.37	0.02	0.00	0.00
Lorentz	10.6	0.91	0.77	0.64	0.52	0.21	0.08	0.03
MPD	20.6	0.92	0.76	0.57	0.39	0.04	0.00	0.00
λ = 12								
expt	6.0	0.97	0.93	0.88	0.82	0.60	0.40	0.23
Gauss	11.6	0.98	0.93	0.86	0.76	0.36	0.11	0.02
Lorentz	4.4	0.97	0.93	0.88	0.83	0.61	0.43	0.29
MPD	11.1	0.98	0.93	0.86	0.77	0.38	0.12	0.03
λ = 20								
expt	4.4	0.98	0.95	0.91	0.87	0.72	0.56	0.45
Gauss	10.1	0.98	0.95	0.89	0.82	0.46	0.18	0.05
Lorentz	3.8	0.98	0.95	0.90	0.86	0.66	0.49	0.36
MPD	9.9	0.98	0.95	0.89	0.82	0.47	0.19	0.06

[a] Full-width at half-height for the 002 reflection.

tion, using the measured $\langle P_2 \rangle$ and $\langle P_4 \rangle$ values as fitting parameters. Bower has proposed such a function, the "most probable distribution" (MPD), which was found to correspond reasonably well to the observed distributions for low density polyethylene at draw ratios below 4.[40] Other authors have assumed that the molecular orientation distribution has a Gaussian shape,[15,41] such as Spiess, who has developed a method enabling the calculation of any $\langle P_n \rangle$ coefficient from ^{2}H NMR measurements.[15]

Table III compares some of the $\langle P_n \rangle_c$ coefficients that were calculated for the molecular orientation distribution in λ = 6, 12, and 20 samples with coefficients calculated by using Gaussian, Lorentzian, and Bower's MPD functions. These functions are defined by the equations

$$\text{Gaussian} \qquad N(\chi) = \exp[-(\chi/a)^2] \tag{12}$$

$$\text{Lorentzian} \qquad N(\chi) = [1 + (\chi/a)^2]^{-2} \tag{13}$$

$$\text{MPD} \qquad N(\chi) = \exp[\alpha_0 + \alpha_2 P_2(\cos\chi) + \alpha_4 P_4(\cos\chi)] \tag{14}$$

where a, α_0, α_2, and α_4 are the parameters controlling the width of the distribution, which in all cases is centered at $\chi = 0°$. For each set of experimental $\langle P_n \rangle_c$ coefficients, the adjustable parameters of the distribution functions were varied in order to obtain the best fit between the experimental and calculated $\langle P_2 \rangle_c$ and $\langle P_4 \rangle_c$ values.

For all samples the Gaussian and MPD functions give $\langle P_n \rangle_c$ coefficients that are below those obtained from experiment for $n \geq 6$ (Table III). Since the $\langle P_2 \rangle_c$ and $\langle P_4 \rangle_c$ values are used as fitting parameters, the $\langle P_6 \rangle_c$ value obtained from these distributions is not very far from those calculated from the X-ray data, but the discrepancy increases rapidly with n. This poor correlation is related to the width of the mathematical distributions with respect to the experimental peaks. If their full-widths at half-height are made equal to the experimental ones, Gaussian and MPD distributions give $\langle P_n \rangle_c$ coefficients much larger than those calculated from the experimental curves, because the exponential form of these two functions causes a very rapid decrease of $N(\chi)$ as the polar angle increases. The main difference between these calculated curves and the experimental ones thus lies in the absence of a low intensity tail in the distribution, which is observed experimentally. It may be noticed in Table III that the results obtained for the λ = 6 sample give a better fit with the Gaussian and MPD functions than those calculated at higher draw ratios. This seems to indicate that this type of relationship gives an acceptable approximation of the orientation distribution at low draw ratios, as shown by Bower, but the quality of the agreement with the experimental results deteriorates at higher deformation. It is seen in Table III that the Lorentzian distribution offers a better correlation with the experimental $\chi_{1/2}$ and $\langle P_n \rangle_c$ values than the two-exponential relations. The $\langle P_n \rangle_c$ coefficients calculated with the Lorentzian function are higher than the experimental ones for the λ = 6 sample and lower in the case of the λ = 20 sample, while the two sets of values are very similar at λ = 12.

These results show that it may not be possible to reproduce the shape of the molecular orientation distribution using a simple relationship. In order to verify this assumption, some curve-fitting calculations were made, using Gaussian or Lorentzian functions, by an addition or a product of these functions.[42] The results obtained with the 002 polar scans of the λ = 12, 16, and 20 samples indicate that the shape of the peaks is best reproduced by the addition of two curves, each being a sum of a Gaussian and a Lorentzian, with a major peak of approximately Gaussian shape and a minor Lorentzian one. This could also be taken as an indication of the presence of two different populations of crystals in the WAXD analysis.

Conclusions

WAXD measurements made on extruded HDPE rods have shown that the molecular orientation of the crystalline phase still increases at the higher draw ratios (λ = 20), even if the $\langle P_2 \rangle$ coefficient has already reached a constant value ($\langle P_2 \rangle \geq 0.98$ at $\lambda \geq 12$).

It is possible to follow the evolution of this orientation by using the higher $\langle P_n \rangle$ coefficients (up to n = 32 in the present work). These coefficients are useful not only to indicate the degree of orientation but also to define the shape of the orientation distribution and the position of its maximum.

For samples of cylindrical symmetry, the $\langle P_n \rangle_c$ coefficients, which describe the orientation distribution of the molecular chains, may be obtained from any crystalline reflection, although for mathematical reasons $hk0$ or $00l$ planes give the best results.

A comparison of the average experimental $\langle P_n \rangle_c$ coefficients with those calculated from the pseudoaffine model

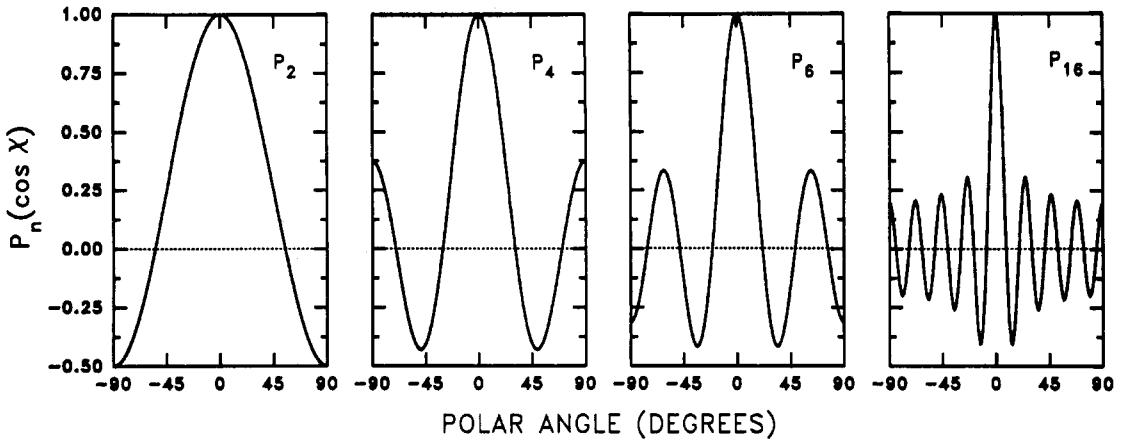

Figure 12. Curves of the Legendre polynomials, $P_n(\cos \chi)$, for n = 2, 4, 6, and 16.

Table IV
$\langle P_n \rangle$ Coefficients Obtained for the 020 and 002 Reflections with the λ = 12 Sample Using Different Calculation Procedures

reflectn	integratn range,[a] deg	integrated intensity[b]	$\langle P_n \rangle$						
			n = 2	n = 4	n = 6	n = 8	n = 16	n = 24	n = 32
020	0–90	53.9	−0.42	0.33	−0.26	0.21	0.11	0.06	0.03
	45–90	50.9	−0.48	0.34	−0.27	0.22	0.12	0.07	0.04
	45–90 S	49.8	−0.49	0.35	−0.27	0.23	0.12	0.07	0.04
002	0–90	23.9	0.32	0.35	0.43	0.35	0.24	0.19	0.11
	0–40	11.0	0.96	0.88	0.80	0.73	0.54	0.36	0.22
	0–40 S	10.5	0.97	0.91	0.84	0.78	0.57	0.38	0.24

[a] Calculations made with smoothed intensity curves are indicated by an "S". [b] Sine-weighted integrated intensity computed in the specified angular range.

demonstrates that this model does not describe adequately the evolution of the molecular orientation in the crystalline phase. Moreover, the agreement between the measured orientation distributions and Gaussian or Bower's most probable distributions is not adequate, the correlation being better using curves of Lorentzian shape.

Acknowledgment. This work was made possible through financial support from the Natural Sciences and Engineering Research Council of Canada and the Alcan International Co. We also thank the Polymer Research Group of the Alcan R&D Centre in Kingston (Ontario, Canada) for the preparation of the HDPE cylindrical rods used in this study.

Appendix

Characteristics of the Legendre Polynomials. Curves of Legendre polynomials of degree n = 2, 4, 6, and 16 are plotted in Figure 12. As the molecular orientation distributions exhibit mirror symmetry with respect to the plane perpendicular to the deformation direction, the calculations need to be performed in one quadrant only (χ = 0–90°). This leads to a series containing the even coefficients only, the odd $\langle P_n \rangle$ coefficients being equal to zero. The $P_0(\cos \chi)$ polynomial has a value of unity at any polar angle and is thus characteristic of an isotropic distribution. All other polynomials possess a maximum equal to unity at χ = 0° and an extremum at χ = 90°, which is positive for even $n/2$ values and negative for odd $n/2$ values. The Legendre polynomial curves show an alternance of positive and negative lobes, the value of the polynomial changing sign $n/2$ times in the χ = 0–90° range. It can also be noticed that the main lobe centered at χ = 0° is somewhat broader than the other lobes.

In the calculation of $\langle P_n \rangle$ coefficients through eq 5, the experimental intensity peak is compared to the polynomial curve. For a peak of width W located at an angle χ_0, the $\langle P_n \rangle$ coefficient will tend toward the value of the polynomial at this position when the width of the peak narrows down:

$$\lim_{W \to 0} \langle P_n \rangle = P_n(\cos \chi_0) \qquad \text{(A1)}$$

For a narrow peak that coincides with an extremum of the polynomial, as is the case for meridional (00l) and equatorial (hk0) reflections, the $\langle P_n \rangle$ values are close to the extremum value. For example, the $\langle P_2 \rangle_c$ values obtained with highly oriented polymers are very close to unity, because the $P_2(\cos \chi)$ curve is very broad with respect to the molecular orientation distribution in these samples. However, when the experimental orientation distribution is compared to the narrower lobes of the higher polynomials, some part of the peak corresponds to decreasing values of the polynomial, which results in lower $\langle P_n \rangle$ coefficients. Finally, for distributions that are much broader than the lobes of the polynomial, the integral of eq 5 is a sum of positive and negative values obtained from successive lobes and the coefficients tend toward zero.

Calculation Procedure for 020 and 002 $\langle P_n \rangle$ Coefficients. $\langle P_n \rangle$ coefficients calculated by using different procedures with the 020 and 002 polar scans of the λ = 12 sample are listed in Table IV. In order to exclude contributions from the orthorhombic 011 and 111 planes and the monoclinic 001 plane (see Table I and Figure 4), the integration was limited to an angular range between 45 and 90°. The $\langle P_n \rangle_{020}$ values so obtained are in much closer agreement with those obtained from the 110 and 200 planes, as seen in Table II. It can be noticed that the lower $\langle P_n \rangle$ values are more sensitive to this calculation artifact than the higher ones. This can be explained by the shape of the Legendre polynomial curves, which change sign $n/2$ times in the χ = 0–90° interval. For example, the $P_2(\cos \chi)$ values are positive between 0 and 55° and

negative from 55 to 90°. Therefore, the unresolved reflections appearing in the 020 polar scan, which arise between 0 and 45°, lead to $\langle P_2 \rangle$ values that are less negative than expected from the calculations made from other $hk0$ planes. For higher $\langle P_n \rangle$ coefficients, the intensity contribution from the unresolved planes adds up to both the positive and negative lobes of the polynomials and its presence cancels out to a large extent.

For the 002 plane, the important difference between sets of $\langle P_n \rangle$ values obtained in the 0–90° angular range or in restricted intervals shows that the choice of the integration range is critical for this reflection. This difference comes from the sine factor in eqs 4 and 5, which amplifies the unresolved reflections appearing around $\chi = 60$ and 90° in the polar scans, while the 002 peak centered at $\chi = 0°$ is weighted by very small sin χ values. Even if the peak intensity of the unresolved reflections is less than 2% of the 002 maximum intensity, the sine-weighted integrated intensity (denominator of eq 4) in the 45–90° range amounts to half the total 0–90° value. In comparison, the reduction of the integration range of the 020 reflection from 0–90° to 45–90° cuts off less than 5% of the integrated intensity. The $\chi = 0$–40° interval was finally chosen for the $\langle P_n \rangle_{002}$ calculations for all the samples investigated because the 002 intensity falls to the background value inside this range, while the onset of the 231/421/511 peak is located at about 45°.

The smoothing of the polar scan curve has a stronger influence on the $\langle P_n \rangle$ values calculated from the 002 reflection than on those obtained from the other planes. This behavior is also related to the sine factor of eqs 4 and 5, which amplifies the noise in the background. Some experiments made on ultraoriented fibers and films have shown that, for very narrow distributions centered at $\chi = 0°$, the integrated intensity caused by the noise may be comparable to the intensity of the peak under investigation; the smoothing is then critical.[43]

Reproducibility of the Measurements and Uncertainty of $\langle P_n \rangle$ Coefficients. In order to verify the homogeneity of the samples and the reproducibility of the experimental intensity curves, polar scans of the 110, 200, 020, and 002 reflections were made in the center of two different platelets cut from the $\lambda = 6$, 12, and 20 rods. In all cases, the intensity at the peak maximum and the background intensity were reproducible within 5%, and the sine-weighted integrated intensity (the denominator of eq 4) was reproducible within 4%. The difference between $\langle P_n \rangle$ and $\langle P_n \rangle_c$ values, calculated from a given plane, for two different platelets and using similar calculation parameters was at most 0.01. Moreover, the cylindrical symmetry of the orientation distribution of the crystal axis with respect to the extrusion direction was verified by studying two platelets cut along diameters of a rod that were perpendicular to one another.

References and Notes

(1) Roe, R. J.; Krigbaum, W. R. *J. Chem. Phys.* **1964**, *40*, 2608.
(2) Krigbaum, W. R.; Roe, R. J. *J. Chem. Phys.* **1964**, *41*, 737.
(3) Roe, R. J. *J. Appl. Phys.* **1965**, *36*, 2024.
(4) Matsuo, M.; Hirota, K.; Fujita, K.; Kawai, H. *Macromolecules* **1978**, *11*, 1000.
(5) Fujita, K.; Suehiro, S.; Nomura, S.; Kawai, H. *Polym. J.* **1982**, *14*, 545.
(6) Krigbaum, W. R.; Adachi, T.; Dawkins, J. V. *J. Chem. Phys.* **1968**, *49*, 1532.
(7) Krigbaum, W. R.; Balta, Y. I. *J. Phys. Chem.* **1967**, *71*, 1770.
(8) Hermans, J. J.; Hermans, P. H.; Vermaas, D.; Weidinger, A. *Recl. Trav. Chim. Pays-Bas* **1946**, *65*, 427.
(9) Hermans, P. H. *Contribution to the Physics of Cellulose Fibers*; Elsevier: Amsterdam, The Netherlands, 1946.
(10) Wilchinsky, Z. W. *J. Appl. Phys.* **1959**, *30*, 792.
(11) Wilchinsky, Z. W. *Adv. X-Ray Anal.* **1962**, *6*, 231.
(12) Sack, R. A. *J. Polym. Sci.* **1961**, *54*, 543.
(13) Peterlin, A. *Colloid Polym. Sci.* **1987**, *265*, 357.
(14) McBrierty, V. J.; McDonald, I. R.; Ward, I. M. *J. Phys. D: Appl. Phys.* **1971**, *4*, 88.
(15) Hentschel, R.; Sillescu, H.; Spiess, H. W. *Polymer* **1981**, *22*, 1516.
(16) Lovell, R.; Mitchell, G. R. *Acta Crystallogr.* **1981**, *A37*, 135.
(17) Bunn, C. W. *Trans. Faraday Soc.* **1939**, *35*, 482.
(18) Walter, E. R.; Reding, F. P. *J. Polym. Sci.* **1956**, *21*, 561.
(19) Swan, P. R. *J. Polym. Sci.* **1962**, *56*, 403.
(20) Takahashi, Y.; Ishida, T.; Furusaka, M. *J. Polym. Sci., Polym. Phys. Ed.* **1988**, *26*, 2267.
(21) Seto, T.; Hara, T.; Tanaka, K. *Jpn. J. Appl. Phys.* **1968**, *7*, 31.
(22) Deas, H. D. *Acta Crystallogr.* **1952**, *5*, 542.
(23) Tallqvist, H. *Acta Soc. Sci. Fenn., Ser. A* Sechsstelige Tafeln der 32 Ersten Kugelfunktionen $P_n(\cos \theta)$. **1938**.
(24) Wilchinsky, Z. W. *J. Polym. Sci., Polym. Phys. Ed.* **1968**, *6*, 281.
(25) Stein, R. S. *J. Polym. Sci.* **1959**, *34*, 709.
(26) Pietralla, M. *Colloid Polym. Sci.* **1976**, *254*, 249.
(27) Stein, R. S.; Norris, F. H. *J. Polym. Sci.* **1956**, *21*, 381.
(28) Gupta, V. B.; Keller, A.; Ward, I. M. *J. Macromol. Sci. Phys.* **1968**, *B2*, 139.
(29) Desper, C. R. *J. Macromol. Sci. Phys.* **1973**, *B7*, 105.
(30) Kratky, O. *Kolloid Z.* **1933**, *64*, 213.
(31) Nomura, S.; Kawai, H.; Kimura, I.; Kagiyama, M. *J. Polym. Sci., Polym. Phys. Ed.* **1970**, *8*, 383.
(32) Nomura, S.; Nakamura, N.; Kawai, H. *J. Polym. Sci., Polym. Phys. Ed.* **1971**, *9*, 407.
(33) Heise, B.; Kilian, H. G.; Pietralla, M. *Prog. Colloid Polym. Sci.* **1977**, *62*, 16.
(34) Nobbs, J. H.; Bower, D. I.; Ward, I. M. *Polymer* **1976**, *17*, 25.
(35) Nobbs, J. H.; Bower, D. I.; Ward, I. M. *J. Polym. Sci., Polym. Phys. Ed.* **1979**, *17*, 259.
(36) Unwin, A. P.; Bower, D. I.; Ward, I. M. *Polymer* **1985**, *26*, 1605.
(37) Bower, D. I.; Jarvis, D. A.; Ward, I. M. *J. Polym. Sci., Polym. Phys. Ed.* **1986**, *24*, 1459.
(38) Ward, I. M. *Adv. Polym. Sci.* **1985**, *66*, 82.
(39) Windle, A. H. In *Developments in Oriented Polymers*; Ward, I. M., Ed.; Applied Science Publishers: London, 1982; Chapter I.
(40) Bower, D. I. *J. Polym. Sci., Polym. Phys. Ed.* **1981**, *19*, 93.
(41) Wu, W.; Simpson, P. G.; Black, W. B. *J. Polym. Sci., Polym. Phys. Ed.* **1980**, *18*, 751.
(42) Note: These calculations were conducted by using the SQUARE TOOLS programs (Spectrum Square Associates Inc.) in the Spectra Calc environment (Galactic Industries Corp.).
(43) Debigaré, J.; Lafrance, C. P.; Prud'homme, R. E., to be published.

Registry No. SCLAIR 2909, 9002-88-4.